EURASIP Journal on Applied Signal Processing 2002:1, 73–79

Construction of Nonseparable Multiwavelets for Nonlinear Image Compression

Ana M. C. Ruedin

Departamento de Computación, Facultad de Ciencias Exactas y Naturales, Universidad de Buenos Aires, Argentina
Email: anita@dc.uba.ar

Received 31 July 2001 and in revised form 2 November 2001

A procedure for the construction of balanced orthogonal nonseparable quincunx multiwavelets, having filters with good lowpass properties, is introduced. The matrix filter bank is viewed as the polyphase matrix of other filters, upon which the lowpass condition is imposed. The multiscaling functions obtained are plotted by means of the cascade algorithm. The process of transforming an image with these wavelets is outlined: formulae for analysis and synthesis are given, the first steps are illustrated with images, and the decomposition of the original image into two input images is addressed. Compression is achieved in a nonlinear process. Experimental results show that (i) the constructed multiwavelets having lowpass properties perform better than other nonseparable multiwavelets, (ii) the energy compaction in the fine detail subbands is greater for the multiwavelets than for the one-dimensional wavelets tried.

Keywords and phrases: multiwavelets, nonseparable, quincunx, polyphase, balanced.

1. INTRODUCTION

In the last 15 years wavelets have been an expanding research field, with many applications such as image compression, image denoising, and pattern recognition, among others. They have proved very efficient in image compression: they have good time-frequency localization, they decorrelate the data and give a sparse representation of the image.

Multiwavelets are a generalization of the wavelet theory. They exploit the spatial correlations between various input images, such as multitemporal images. They can be designed to have several suitable properties simultaneously, such as orthogonality, polynomial approximation, short support and symmetry, see [1, 2, 3, 4, 5]. They have given good results for signal compression, see [6, 7, 8, 9]. In order to apply multiwavelets, either the input data must be prefiltered (see [10, 11, 12, 13, 14]) or the multiwavelets themselves must be balanced (see [15, 16]).

Nonseparable wavelets have been introduced and investigated, and examples have been given in [17, 18, 19]. This is a more general setting than the classical one, nonseparable filters are used, and decimation is achieved with a dilation matrix. In this way the errors of thresholding the transformed coefficients do not lie mainly in the horizontal and vertical directions—which does not agree with our visual system.

In an attempt to unify advances made in both directions: multiwavelets, and nonseparable bidimensional wavelets, examples were built of continuous, nonseparable, orthogonal multiscaling functions in [20]. They are compactly supported, have quincunx decimation, and have polynomial approximation orders (i.e., accuracy) 2 and 3. Their corresponding multiwavelets were also found. In [21] other examples were given, with the additional property of being balanced.

In this work we construct multiwavelets that are balanced, continuous, nonseparable, orthogonal, have quincunx decimation, have accuracy 2 or 3, and whose filters have good lowpass properties, in order to give more energy compaction. Their coefficients are given in the appendix. In Section 2 some general concepts and notation are given. In Section 3 the process of the multiwavelet transform of an image is outlined for these wavelets. Formulae for analysis and synthesis are given. The first steps are illustrated with images. The decomposition of the original image into 2 input images is addressed in Section 4. In Section 5 we show how the multiwavelets are obtained, by imposing lowpass conditions. In Section 6 we explain how compression is achieved in a nonlinear process: this nonlinearity is not the result of the application of a nonlinear operator, but the result of thresholding the coefficients obtained by a linear operator—the multiwavelet transform. We also give several experimental results, comparing the performance of the constructed multiwavelets to that of other nonseparable multiwavelets, and to well-known one-dimensional wavelets. Concluding remarks are in Section 7.

2. NONSEPARABLE ORTHOGONAL QUINCUNX MULTIWAVELETS

Let Φ_1 and Φ_2 be two continuous scaling functions defined over $\mathbb{R}^2$ such that the family $\{\Phi_1(x-k), \Phi_2(x-l)\}$ is

orthonormal. In vector form the dilation equation becomes

$$\Phi(x) = \sum_{k\in\Lambda\subset\mathbb{Z}^2} H^{(k)}\Phi(Dx-k),$$
$$\begin{bmatrix}\Phi_1(x)\\ \Phi_2(x)\end{bmatrix} = \sum_k \left[H^{(k)}\right]\begin{bmatrix}\Phi_1(Dx-k)\\ \Phi_2(Dx-k)\end{bmatrix}, \tag{1}$$

where $H^{(k)}$ are 2×2 matrices of a matrix filter bank with indices such as

$$M_0 = \begin{bmatrix} 0 & H^{(1,1)} & H^{(2,1)} & 0\\ H^{(0,0)} & H^{(1,0)} & H^{(2,0)} & H^{(3,0)}\\ 0 & H^{(1,-1)} & H^{(2,-1)} & 0\end{bmatrix} \tag{2}$$

and D is the dilation matrix. Notation is simplified and $\Phi_1(Dx-k)$ means that we apply Φ_1 to the two components of $Dx-k = \left[\begin{smallmatrix} d_{11} & d_{12}\\ d_{21} & d_{22}\end{smallmatrix}\right]\left[\begin{smallmatrix} x_1\\ x_2\end{smallmatrix}\right] - \left[\begin{smallmatrix} k_1\\ k_2\end{smallmatrix}\right]$. We consider two possible dilation matrices: D_1, a reflection followed by an expansion of $\sqrt{2}$, and D_2, a rotation followed by an expansion of $\sqrt{2}$. For both matrices $|D| = |\det(D)| = 2$,

$$D_1 = \begin{bmatrix}1 & 1\\ 1 & -1\end{bmatrix}, \qquad D_2 = \begin{bmatrix}1 & -1\\ 1 & 1\end{bmatrix}. \tag{3}$$

Both D_1 and D_2 induce a decomposition of the sets of all pairs of integers $\mathbb{Z}^2$ into two cosets: Γ_1 and Γ_2, forming the quincunx sublattices—black and white squares of a chess-table:

$$\mathbb{Z}^2 = \Gamma_1\cup\Gamma_2; \quad \Gamma_1 = \{D\mathbb{Z}^2\}; \quad \Gamma_2 = \left\{D\mathbb{Z}^2 + \begin{bmatrix}1\\0\end{bmatrix}\right\}. \tag{4}$$

The number of wavelets is $|D|-1 = 1$ in both cases. The equation for the multiwavelet, in vector form, is

$$\Psi(x) = \sum_k G^{(k)}\Phi(Dx-k). \tag{5}$$

Finally we recall some general notation. Given a 2d filter F, the $\mathbb{Z}$ transform of F is

$$F(z_1,z_2) = \sum_{(j,k)\in\mathbb{Z}^2} F_{jk}z_1^{-j}z_2^{-k}, \tag{6}$$

and the frequency response of F is

$$\hat{F}(w_1,w_2) = \sum_{(j,k)\in\mathbb{Z}^2} F_{jk}e^{-i(w_1 j + w_2 k)}. \tag{7}$$

Given a 2d signal x, we define $x\downarrow D$ (x downsampled with D) as

$$y = x\downarrow D \Longleftrightarrow y_n = x_{Dn}. \tag{8}$$

3. ANALYSIS SYNTHESIS FORMULAE

Assume that we decompose the original image $X^{(0)}$ into two input images $c_{1,k}^{(0)}$ and $c_{2,k}^{(0)}$ ($k\in\mathbb{Z}^2$), and let $f(x)$ be the function that verifies

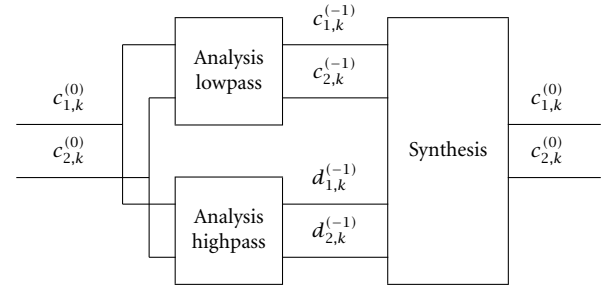

Figure 1: Analysis-synthesis scheme.

$$f\in V_0 = \operatorname{span}\{\Phi_1(\cdot-k),\Phi_2(\cdot-l)\}_{k,l\in\mathbb{Z}^2},$$
$$f(x) = \sum_{k\in\mathbb{Z}^2}\left(c_{\cdot,k}^{(0)}\right)^T\Phi(x-k), \quad \text{where } c_{\cdot,k}^{(0)} = \begin{bmatrix}c_{1,k}^{(0)}\\ c_{2,k}^{(0)}\end{bmatrix}. \tag{9}$$

The analysis scheme (see Figure 1) outputs two approximation images $c_{1,k}^{(-1)}$ and $c_{2,k}^{(-1)}$, and two detail images $d_{1,k}^{(-1)}$ and $d_{2,k}^{(-1)}$. We set

$$c_{\cdot,k}^{(-1)} = \begin{bmatrix}c_{1,k}^{(-1)}\\ c_{2,k}^{(-1)}\end{bmatrix}, \qquad d_{\cdot,k}^{(-1)} = \begin{bmatrix}d_{1,k}^{(-1)}\\ d_{2,k}^{(-1)}\end{bmatrix}. \tag{10}$$

We have

$$V_0 = V_{-1}\oplus W_{-1}, \quad V_{-1}\perp W_{-1}, \tag{11}$$

where

$$V_{-1} = \operatorname{span}\{\Phi_1(D^{-1}\cdot-k),\Phi_2(D^{-1}\cdot-l)\}_{k,l\in\mathbb{Z}^2},$$
$$W_{-1} = \operatorname{span}\{\Psi_1(D^{-1}\cdot-k),\Psi_2(D^{-1}\cdot-l)\}_{k,l\in\mathbb{Z}^2}. \tag{12}$$

Writing $f(x)$ as the sum of its projections onto V_{-1} and W_{-1}

$$f(x) = \frac{1}{\sqrt{|D|}}\sum_{k\in\mathbb{Z}^2} c_{\cdot,k}^{(-1)T}\Phi(D^{-1}x-k) + \frac{1}{\sqrt{|D|}}\sum_{k\in\mathbb{Z}^2} d_{\cdot,k}^{(-1)T}\Psi(D^{-1}x-k), \tag{13}$$

it can be shown that the *analysis formulae* are

$$c_k^{(-1)} = \frac{1}{\sqrt{|D|}}\sum_{j\in\mathbb{Z}^2} H^{(j-Dk)}\,c_{\cdot,j}^{(0)}, \tag{14}$$

$$d_k^{(-1)} = \frac{1}{\sqrt{|D|}}\sum_{j\in\mathbb{Z}^2} G^{(j-Dk)}c_{\cdot,j}^{(0)}. \tag{15}$$

Similarly, it can be shown that the *synthesis formula* is

$$c_k^{(0)} = \frac{1}{\sqrt{|D|}}[U_k + V_k], \tag{16}$$

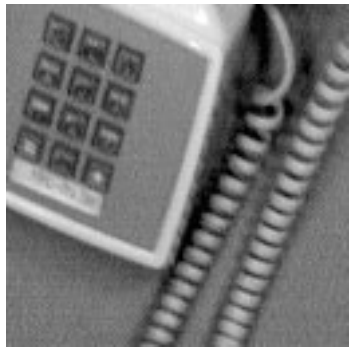

Figure 2: Original image.

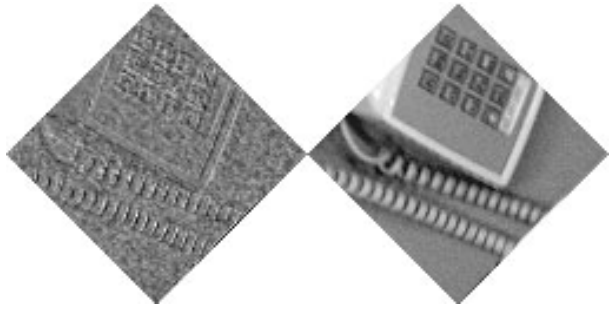

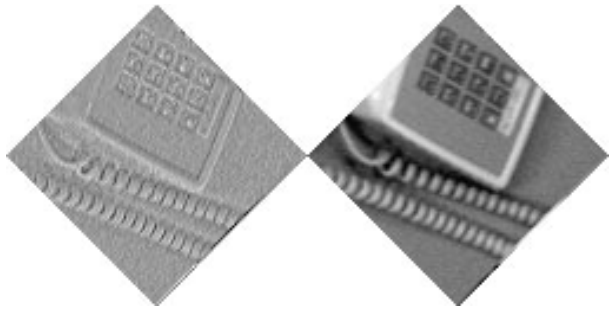

Figure 3: One step of the multiwavelet transform.

where

$$U_k = \sum_{j\in\mathbb{Z}^2} \left(H^{(k-Dj)}\right)^T c_{\cdot,j}^{(-1)},$$
$$V_k = \sum_{j\in\mathbb{Z}^2} \left(G^{(k-Dj)}\right)^T d_{\cdot,j}^{(-1)}. \tag{17}$$

In Figure 2 we have a phone, the original image. We copy the image to begin with and take $c_{1,\cdot}^{(0)} = c_{2,\cdot}^{(0)} = X^{(0)}$.

In Figure 3 we have 4 images, they are the coefficients of one step of the multiwavelet transform $d_{1,\cdot}^{(-1)}$ (top left), $c_{1,\cdot}^{(-1)}$ (top right) and $d_{2,\cdot}^{(-1)}$ (bottom left), $c_{2,\cdot}^{(-1)}$ (bottom right). The dilation matrix was D_1. The effect of downsampling with D_1 in the analysis formula is to reflect and contract the image.

In Figure 4 we have the coefficients of two steps of the same transform: $d_{1,\cdot}^{(-1)}$, $d_{1,\cdot}^{(-2)}$, $c_{1,\cdot}^{(-2)}$ (top) and $d_{2,\cdot}^{(-1)}$, $d_{2,\cdot}^{(-2)}$, $c_{2,\cdot}^{(-2)}$ (bottom). After two steps the image has recovered its original orientation. It takes four steps to do so if the dilation matrix is D_2.

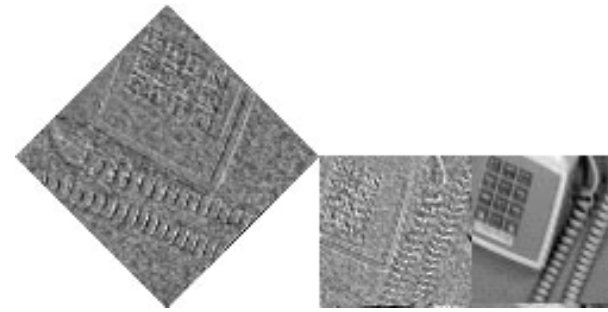

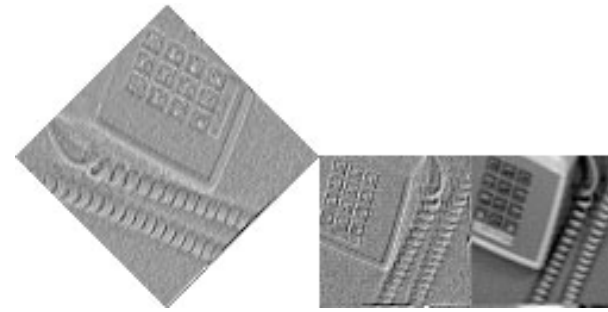

Figure 4: Two steps of the multiwavelet transform.

At each step, before the images are processed they have to be periodized, otherwise there are artifacts at the borders. Periodization is different if the frames of the images are normally oriented squares (after the even steps) or diamond-oriented squares (after the odd steps).

4. ONE INPUT IMAGE DECOMPOSED INTO TWO INPUT IMAGES

At the beginning of the process the original image may be copied so as to get two input images, but duplicating the input signal will not help for compression.

One squared image is not divided straightforwardly into two squared images. Notice, however, that after one step of the analysis procedure we get two diamond-like matrices of approximation coefficients, and each one has half the size of the original image. Therefore, we decompose the original image into two diamonds. We might build one diamond by cutting out the corners of the original image, and build the other with the rest, but the algorithm (14) mixes information from the two images and this gives poor results for compression. The two input images should be alike, this we manage by separating into two diamonds the pixels belonging to each coset (see Figure 5).

Notice that in this way all the coefficients of the multiwavelet transform need as much storage as the original image, and can be made to fit into it.

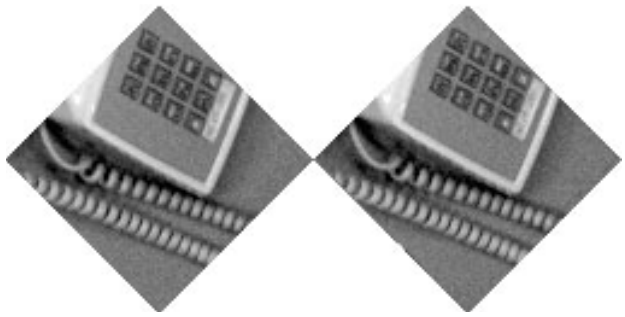

Figure 5: Pixels in first (left) and second (right) cosets of original phone.

5. CONSTRUCTION OF MULTIWAVELETS

In [21] the properties of orthogonality, accuracy and balancing were analyzed, and for each property were derived conditions for the matrix filter coefficients $H^{(k)}$. The conditions for accuracy or polynomial approximation order were obtained from [22]. All the conditions helped to build examples of different nonseparable multiwavelets, by means of a numerical least-squares optimization routine.

In order to force the filters to have good lowpass properties, we now follow a procedure carried out by Xia [10] in the design of prefilters for 1d multiwavelets. As in the 1d case, a 2×2 matrix filter bank is also a polyphase matrix of two filters (see [23]); the only difference is that here the two filters are two-dimensional.

The approximation coefficients in (14) can be expressed as

$$\begin{aligned} c_{1,\cdot}^{(-1)} &= \frac{1}{\sqrt{|D|}}\left[\left(\tilde{H}_{11}^{(\cdot)} * c_{1,\cdot}^{(0)}\right) + \left(\tilde{H}_{12}^{(\cdot)} * c_{2,\cdot}^{(0)}\right)\right] \downarrow D, \\ c_{2,\cdot}^{(-1)} &= \frac{1}{\sqrt{|D|}}\left[\left(\tilde{H}_{21}^{(\cdot)} * c_{1,\cdot}^{(0)}\right) + \left(\tilde{H}_{22}^{(\cdot)} * c_{2,\cdot}^{(0)}\right)\right] \downarrow D, \end{aligned} \tag{18}$$

where the symbol $*$ denotes discrete 2d convolution, and $\tilde{H}^{(k,l)} = H^{(-k,-l)}$.

Let $c_{1,\cdot}^{(0)}$ be the pixels of the image $X^{(0)}$ on coset Γ_1, and $c_{2,\cdot}^{(0)}$ be the pixels of the image on coset Γ_2. Then

$$\begin{aligned} X^{(0)}(z_1, z_2) &= c_{1,\cdot}^{(0)}(z^D) + z_1 c_{2,\cdot}^{(0)}(z^D), \\ c_{1,\cdot}^{(0)}(z_1, z_2) &= \sum_{n=(j,k)\in\mathbb{Z}^2} X_{Dn}^{(0)} z_1^{-j} z_2^{-k}, \\ c_{2,\cdot}^{(0)}(z_1, z_2) &= \sum_{n=(j,k)\in\mathbb{Z}^2} X_{Dn+(10)}^{(0)} z_1^{-j} z_2^{-k}. \end{aligned} \tag{19}$$

We can write (18) as

$$c_{1,\cdot}^{(-1)} = [y_{1,\cdot}] \downarrow D, \qquad c_{2,\cdot}^{(-1)} = [y_{2,\cdot}] \downarrow D. \tag{20}$$

Now the $\mathbb{Z}$ transform of $y_{1,\cdot}$ and $y_{2,\cdot}$ is

$$\begin{bmatrix} y_{1,\cdot}(z_1, z_2) \\ y_{2,\cdot}(z_1, z_2) \end{bmatrix} = P_{F_1,F_2} \begin{bmatrix} c_{1,\cdot}^{(0)}(z_1, z_2) \\ c_{2,\cdot}^{(0)}(z_1, z_2) \end{bmatrix}, \tag{21}$$

where

$$P_{F_1,F_2} = \frac{1}{\sqrt{|D|}} \begin{bmatrix} H_{11}^{(\cdot)}\left(\frac{1}{z_1}, \frac{1}{z_2}\right) & H_{12}^{(\cdot)}\left(\frac{1}{z_1}, \frac{1}{z_2}\right) \\ H_{21}^{(\cdot)}\left(\frac{1}{z_1}, \frac{1}{z_2}\right) & H_{22}^{(\cdot)}\left(\frac{1}{z_1}, \frac{1}{z_2}\right) \end{bmatrix} \tag{22}$$

is the polyphase matrix for two filters F_1 and F_2. Filter F_1 has coefficients $H_{11}^{(\cdot)}$ on coset Γ_1 and $H_{12}^{(\cdot)}$ on coset Γ_2, while filter F_2 has coefficients $H_{21}^{(\cdot)}$ on coset Γ_2 and $H_{22}^{(\cdot)}$ on coset Γ_2. Writing down the latter, we have

$$\begin{aligned} F_1(z_1, z_2) &= H_{11}^{(\cdot)}(z^D) + z_1 H_{12}^{(\cdot)}(z^D), \\ F_2(z_1, z_2) &= H_{21}^{(\cdot)}(z^D) + z_1 H_{22}^{(\cdot)}(z^D), \end{aligned} \tag{23}$$

where

$$z^D = (z_1^{d_{11}} z_2^{d_{21}}, z_1^{d_{12}} z_2^{d_{22}}). \tag{24}$$

Furthermore, equation (21) is equivalent to

$$\begin{aligned} y_{1,\cdot} &= (X^{(0)} * \tilde{F}_1) \downarrow D, \\ y_{2,\cdot} &= (X^{(0)} * \tilde{F}_2) \downarrow D. \end{aligned} \tag{25}$$

Since there is one downsampling step in (20), the approximation coefficients $c_{1,\cdot}^{(-1)}$ and $c_{2,\cdot}^{(-1)}$ are obtained from a 2d convolution of the original image with $\tilde{F}_1$ and $\tilde{F}_2$ plus two downsampling steps. If we impose the lowpass property

$$\begin{aligned} \hat{\tilde{F}}_1(\pi, \pi) &= \tilde{F}_1(-1, -1) = 0, \\ \hat{\tilde{F}}_2(\pi, \pi) &= \tilde{F}_2(-1, -1) = 0, \end{aligned} \tag{26}$$

we obtain the lowpass polyphase filter condition (for either dilation matrix D_1 or D_2)

$$\sum_{k\in\mathbb{Z}^2} H_{11}^{(k)} = \sum_{k\in\mathbb{Z}^2} H_{12}^{(k)}, \qquad \sum_{k\in\mathbb{Z}^2} H_{21}^{(k)} = \sum_{k\in\mathbb{Z}^2} H_{22}^{(k)}. \tag{27}$$

With a numerical optimization routine, we obtained matrix filter coefficients verifying the above requirement plus all the conditions for orthogonality, accuracy two and balancing. Coefficients are given in the appendix. The two scaling functions were plotted with eight iterations of the cascade algorithm, see Figures 6 and 7.

The corresponding wavelet coefficients $G^{(k)}$ were found in a similar way.

6. COMPRESSION

After the image has been transformed J steps, we have

$$\begin{aligned} f(x) = &\sum_{k\in\mathbb{Z}^2} \left(c_{\cdot,k}^{(-J)}\right)^T |D|^{-J/2} \Phi(D^{-J}x - k) \\ &+ \sum_{j=1}^{J} \sum_{k\in\mathbb{Z}^2} \left(d_{\cdot,k}^{(-j)}\right)^T |D|^{-j/2} \Psi(D^{-j}x - k). \end{aligned} \tag{28}$$

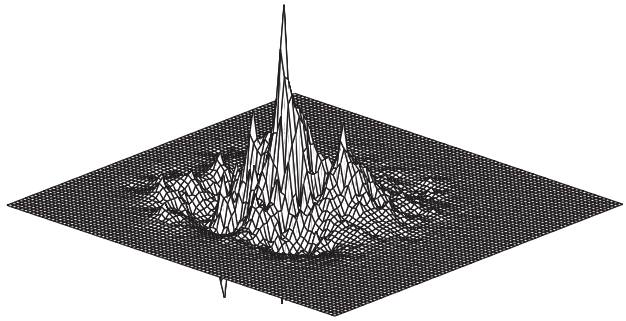

Figure 6: Scaling function 1.

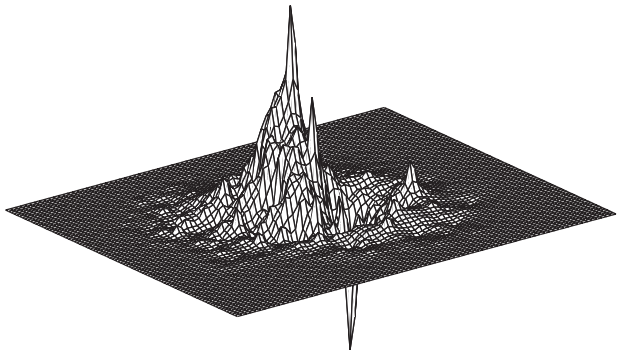

Figure 7: Scaling function 2.

Since the system

$$\begin{aligned}&\Big\{|D|^{-J/2}\Phi_1(D^{-J}x-k),\ |D|^{-J/2}\Phi_2(D^{-J}x-k),\\&|D|^{-J/2}\Psi_1(D^{-J}x-k),\ |D|^{-J/2}\Psi_2(D^{-J}x-k),\\&\ldots,|D|^{-1/2}\Psi_1(D^{-1}x-k),\ |D|^{-1/2}\Psi_2(D^{-1}x-k)\Big\}\end{aligned}\tag{29}$$

is orthonormal, the sums of squares of all the coefficients $c_{1,k}^{(-J)}c_{2,k}^{(-J)}d_{1,k}^{(-J)}d_{2,k}^{(-J)}\cdots d_{1,k}^{(-1)}d_{2,k}^{(-1)}$ is equal to the sums of squares of the original coefficients $\{c_{1,k}^{(0)}c_{2,k}^{(0)}\}$. This means that an error in the transformed coefficients is equal to the error in the reconstructed image (in 2-norm). Suppose we fix the number of coefficients to be kept, and discard the rest. Then keeping the largest transformed coefficients in absolute value, and sending the smaller ones to zero, that is, applying a threshold, is a nonlinear process that minimizes the 2-norm error.

With the filter coefficients $H^{(k)}$ and $G^{(k)}$ of the examples found previously, the multiwavelet transforms were applied to three test images: Lena (256×256), Cameraman (256×256), and Phone (128×128). The number of steps taken was such that the final coarse approximation matrices were of size 8×8. The original images were compressed retaining in all cases 15% of the largest transformed coefficients in absolute value, that is, they will all have the same compression rate as a rough estimate. We list the PSNR in Table 1. The wavelets are named according to their properties: (D_2 – acc3 – bal) means a balanced multiwavelet of accuracy 3 with dilation matrix D_2. Results improved with the order of accuracy of the wavelets; that is, for higher polynomial approximation order, the PSNR was higher, and therefore the MSE was smaller. We can also observe that for wavelets having the same accuracy, those having the polyphase lowpass filter property (LP) have a superior performance. At this stage it is difficult to predict what the final compression rates will be, but since multiwavelets are generalizations of wavelets, we think that these results may be improved by imposing more conditions in the construction of the multiwavelets.

Table 1: PSNR of reconstruction with 15% coefficients.

	PSNR (dB)		
Quincunx Multiwavelet	Lena	Camer	Phone
D_1 – acc1 – bal	30.52	30.94	27.18
D_1 – acc2 – bal	30.80	31.08	28.28
D_2 – acc2 – bal	32.01	31.85	28.28
D_1 – acc3 – bal	31.89	32.20	29.19
D_2 – acc3 – bal	32.54	32.48	28.95
D_1 – acc1 – bal – LP	30.87	32.06	28.57
D_2 – acc2 – bal – LP	32.62	32.50	29.41

Figure 8: Original Cameraman (detail).

Figure 9: Reconstruction with 15% coefficients.

In Figure 8 we have the original Cameraman (detail) and in Figure 9 the reconstructed Cameraman (detail) with a balanced multiwavelet of accuracy 2 with dilation matrix D_2 and lowpass polyphase filter property (D_2 – acc2 – bal – LP) after retaining 15% of the largest coefficients of the multiwavelet transform.

We now present a comparison between the energy com-

Table 2: Energy compaction ratio.

Image Lena	
Wavelet	r
Haar	0.0230
Daubechies 4	0.0178
Biorthogonal 9/7	0.0137
D_2 − acc3 − bal	0.0095
D_2 − acc2 − bal − LP	0.0084

paction (in the fine detail subbands) of three well-known 1d wavelets and that of two multiwavelets. Image Lena was transformed with (i) Haar separable wavelet, (ii) Daubechies four separable wavelet, (iii) Biorthogonal symmetric 9/7 separable wavelet, (iv) multiwavelet D_2 − acc2 − bal − LP, and (v) multiwavelet D_2 − acc3 − bal. The number of steps taken, J, was such that there were 64×64 approximation coefficients: this means $J = 2$ for the separable wavelets, and $J = 4$ for the multiwavelets. We define the energy compaction ratio r as the energy of the detail coefficients divided by the total energy of the transform. We call this ratio r_{MW} for the multiwavelet and r_W for the wavelet.

$$r_{MW} = \frac{\sum_{j=1}^{4}\sum_{i=1}^{2}\sum_{k\in\mathbb{Z}^2}\left(d_{i,k}^{(-j)}\right)^2}{\sum_{j=1}^{4}\sum_{i=1}^{2}\sum_{k\in\mathbb{Z}^2}\left(d_{i,k}^{(-j)}\right)^2+\sum_{i=1}^{2}\sum_{k\in\mathbb{Z}^2}\left(c_{i,k}^{(-4)}\right)^2}, \tag{30}$$

$$r_W = \frac{\sum_{j=1}^{2} E_D^{(-j)}}{\sum_{j=1}^{2} E_D^{(-j)} + E_A^{(-2)}}, \tag{31}$$

where

$$\begin{aligned} E_D^{(-j)} &= \sum_{k\in\mathbb{Z}^2}\left(LH_k^{(-j)}\right)^2+\left(HL_k^{(-j)}\right)^2+\left(HH_k^{(-j)}\right)^2, \\ E_A^{(-2)} &= \sum_{k\in\mathbb{Z}^2}\left(LL_k^{(-2)}\right)^2, \end{aligned} \tag{32}$$

LH, HL, HH (low-high, high-low, and high-high) is the usual notation for the detail coefficients of a separable wavelet, and LL (low-low) stands for the approximation coefficients.

Although formulae (30) and (31) look different, they are conceptually the same, they correspond to the energy of the fine detail subbands divided by the energy of all the wavelet coefficients. For example, in the case of Lena (256×256), in (30) the numerator has the sums of squares of $2(128^2 + 128^2/2 + 64^2 + 64^2/2) = 61440$ fine detail coefficients. The numerator in (31) has the same amount: it corresponds to the sums of squares of $3(128^2 + 64^2) = 61440$ fine detail coefficients.

Observe in Table 2 that the energy compaction ratio is lower for the multiwavelets. This indicates that the fine detail subbands keep little information, and that most of the information is concentrated in the approximation coefficients: if the coefficients are thresholded, we obtain many zeros in the fine detail subbands, which is good for compression. An appropriate coder should contemplate handling zerotrees codification for these multiwavelets.

7. CONCLUSIONS

A procedure for the construction of orthogonal nonseparable multiwavelets with quincunx decimation and lowpass polyphase filter properties has been given. The multiwavelets obtained are balanced and have different polynomial approximation orders. A graph of the two scaling functions associated to one multiwavelet has been obtained by means of a cascade algorithm, and the coefficients are given.

We have shown how image processing is achieved with these wavelets, how the original image is decomposed into two input images, we have given the analysis-synthesis formulae and illustrated the first steps of these transforms.

Once the image has been transformed, the coefficients are thresholded for compression. Experimental results show that for a same compression rate, image quality is higher for the multiwavelets wavelets having higher polynomial approximation order. And that for the same polynomial approximation order, the performance of the wavelets having low-pass properties is superior to the other multiwavelets.

Numerical results also indicate that the energy compaction in the fine detail subbands may be greater for the constructed multiwavelet transforms than for the conventional discrete wavelet transforms. This makes the multiwavelets a potential tool for image or video compression.

APPENDIX

$$H^{(1,1)} = \begin{bmatrix} -2.592566632745038e{-}2 & 3.744699178489502e{-}2 \\ 1.323963014313383e{-}1 & -5.402518841109086e{-}2 \end{bmatrix}$$

$$H^{(2,1)} = \begin{bmatrix} -6.871261590512233e{-}2 & -3.082641914034970e{-}1 \\ 3.331300348199493e{-}2 & 8.257433230141883e{-}2 \end{bmatrix}$$

$$H^{(0,0)} = \begin{bmatrix} 9.101779474899736e{-}2 & 1.147594849860903e{-}3 \\ 1.579615799990289e{-}1 & 1.650959000796863e{-}1 \end{bmatrix}$$

$$H^{(1,0)} = \begin{bmatrix} 3.340926666738988e{-}1 & 4.491466458692672e{-}1 \\ 1.031992112251045e{+}0 & 6.843827156738546e{-}1 \end{bmatrix}$$

$$H^{(2,0)} = \begin{bmatrix} 1.001671974143504e{+}0 & 6.889337709218273e{-}1 \\ -5.060233419523893e{-}1 & -2.082196881883916e{-}1 \end{bmatrix}$$

$$H^{(3,0)} = \begin{bmatrix} -2.521252867158303e{-}1 & -1.720458505197366e{-}2 \\ 8.369373186488886e{-}2 & 4.082100790627226e{-}2 \end{bmatrix}$$

$$H^{(1,-1)} = \begin{bmatrix} 5.457525792861077e{-}2 & 1.100177891678567e{-}1 \\ 9.432610211977062e{-}2 & 2.596028291177161e{-}1 \end{bmatrix}$$

$$H^{(2,-1)} = \begin{bmatrix} -1.345941232130003e{-}1 & 3.877598567725661e{-}2 \\ -2.765948963639682e{-}2 & 2.976809087462491e{-}2 \end{bmatrix}$$

$$w = \begin{bmatrix} 1.0 & 1.0 \end{bmatrix}$$

$$u = \begin{bmatrix} -2.590118834952359e{-}2 & -2.721035516546056e{-}1 \end{bmatrix}$$

$$v = \begin{bmatrix} -1.170391652697625e{+}0 & -7.879636384567043e{-}1 \end{bmatrix}$$

$$G^{(1,1)} = \begin{bmatrix} 1.265442752812728e{-}1 & -5.270803250075925e{-}2 \\ -4.014336198897893e{-}2 & -6.465762486853062e{-}3 \end{bmatrix}$$

$$G^{(2,1)} = \begin{bmatrix} 3.431910340295161e{-}2 & 9.056581868305330e{-}2 \\ 4.278074152313938e{-}2 & 2.233397005025604e{-}1 \end{bmatrix}$$

$$G^{(0,0)} = \begin{bmatrix} -1.030244589035089e-1 & 3.684651927019812e-1 \\ 1.076617041914698e-1 & -2.991279828567442e-1 \end{bmatrix}$$

$$G^{(1,0)} = \begin{bmatrix} 6.469317730309792e-1 & -7.240195732995425e-1 \\ -4.378488471119604e-1 & 7.065039887323013e-1 \end{bmatrix}$$

$$G^{(2,0)} = \begin{bmatrix} 6.223429968194491e-1 & -5.990080922886163e-1 \\ 4.911572165652078e-1 & -8.501352143410924e-1 \end{bmatrix}$$

$$G^{(3,0)} = \begin{bmatrix} 1.641760277533065e-1 & -2.467053380405102e-1 \\ 2.474569759125719e-1 & -2.814270072493299e-1 \end{bmatrix}$$

$$G^{(1,-1)} = \begin{bmatrix} -6.616332019405033e-2 & -2.049768622936048e-1 \\ 6.728234504911705e-2 & 1.389896567428485e-1 \end{bmatrix}$$

$$G^{(2,-1)} = \begin{bmatrix} -4.813292879725325e-2 & -8.606585078521337e-3 \\ -1.560286466880401e-1 & 4.600449840297642e-2 \end{bmatrix}$$

REFERENCES

[1] X.-G. Xia and B. W. Suter, "Vector-valued wavelets and vector filter banks," *IEEE Trans. Signal Processing*, vol. 44, no. 3, pp. 508–518, 1996.

[2] W. Lawton, S. Lee, and Z. Shen, "Stability and orthonormality of multivariate refinable functions," *SIAM J. Math. Anal.*, vol. 28, no. 4, pp. 999–1014, 1997.

[3] Q. T. Jiang, "On the design of multifilter banks and orthonormal multiwavelet bases," *IEEE Trans. Signal Processing*, vol. 46, no. 12, pp. 3292–3303, 1998.

[4] J. Y. Tham, L. Shen, S. L. Lee, and H. H. Tan, "A general approach for analysis and application of discrete multiwavelet transforms," *IEEE Trans. Signal Processing*, vol. 48, no. 2, pp. 457–464, 2000.

[5] X.-G. Xia and B. W. Suter, "Multirate filter banks with block sampling," *IEEE Trans. Signal Processing*, vol. 44, no. 3, pp. 484–496, 1996.

[6] V. Strela, *Multiwavelets: Theory and Applications*, Ph.D. thesis, MIT, June 1996.

[7] V. Strela, P. N. Heller, G. Strang, P. Topiwala, and C. Heil, "The application of multiwavelet filter banks to signal and image processing," to appear in IEEE Trans. Image Processing.

[8] G. Plonka and V. Strela, "Construction of multiscaling functions with approximation and symmetry," *SIAM J. Math. Anal.*, vol. 29, no. 2, pp. 481–510, 1998.

[9] T. Xia and Q. T. Jiang, "Optimal multifilter banks: design, related symmetric extension transform and application to image compression," *IEEE Trans. Signal Processing*, vol. 47, no. 7, pp. 1878–1889, 1999.

[10] X.-G. Xia, J. S. Geronimo, D. P. Hardin, and B. W. Suter, "Design of prefilters for discrete multiwavelet transforms," *IEEE Trans. Signal Processing*, vol. 44, no. 1, pp. 25–35, 1996.

[11] M. Cotronei, L. Montefusco, and L. Puccio, "Multiwavelet analysis and signal processing," to appear in *IEEE Trans. on Circuits and Systems II: Analog and Digital Signal Processing, Special ISSUE on Multirate System, Filter Banks, Wavelets, and Applications*.

[12] S. Bacchelli, M. Cotronei, and T. Sauer, "Multifilters with and without prefilters," preprint.

[13] J. T. Miller and C.-C. Li, "Adaptive multiwavelet initialization," *IEEE Trans. Signal Processing*, vol. 46, no. 12, pp. 3282–3291, 1998.

[14] X.-G. Xia, "A new prefilter design for discrete multiwavelet transforms," *IEEE Trans. Signal Processing*, vol. 46, no. 6, pp. 1558–1570, 1998.

[15] J. Lebrun and M. Vetterli, "Balanced multiwavelets: theory and design," *IEEE Trans. Signal Processing*, vol. 46, no. 4, pp. 1119–1125, 1998.

[16] I. W. Selesnick, "Balanced multiwavelet bases based on symmetric FIR filters," in *Proc. SPIE, Wavelet Applications in Signal and Image Processing VII*, vol. 3813, pp. 122–131, 1999.

[17] A. Cohen and I. Daubechies, "Non-separable bidimensional wavelet bases," *Rev. Mat. Iberoamericana*, vol. 9, no. 1, pp. 51–137, 1993.

[18] J. Kovacevic and M. Vetterli, "Non-separable multidimensional perfect reconstruction filter banks and wavelet bases for r^n," *IEEE Transactions on Information Theory*, vol. 38, no. 2, pp. 533–555, 1992.

[19] J. Kovacevic and M. Vetterli, "New results on multidimensional filter banks and wavelets," preprint.

[20] A. M. Ruedin, "Nonseparable orthogonal multiwavelets with two and three vanishing moments on the quincunx grid," in *Proc. SPIE, Wavelet Applications in Signal and Image Processing VII*, vol. 3813, pp. 455–466, 1999.

[21] A. M. Ruedin, "Balanced nonseparable orthogonal multiwavelets with two and three vanishing moments on the quincunx grid," in *Proc. SPIE, Wavelet Applications in Signal and Image Processing VIII*, A. Aldroubi, A. F. Laine, and M. A. Unser, Eds., vol. 4119, pp. 519–527, December 2000.

[22] C. Cabrelli, C. Heil, and U. Molter, "Accuracy of lattice translates of several multidimensional refinable functions," *J. Approx. Theory*, vol. 95, no. 1, pp. 5–52, 1998.

[23] P. P. Vaidyanathan, *Multirate Systems and Filter Banks*, Prentice-Hall, New Jersey, 1993.

Ana M. C. Ruedin received her degree in Computer Science from the Facultad de Ciencias Exactas y Naturales of the University of Buenos Aires in 1972. She is currently working on her PhD thesis. She has been teaching assistant, and is full-time assistant professor in the Computer Science Department, University of Buenos Aires, since 1991. She has taught subjects such as Numerical Methods, Linear Algebra, Eigenvalue Estimation, Finite Differences, Theory of Wavelets and their Numerical Applications, and New Techniques in Data Compression. Her main research interests are image compression, multiwavelets and nonseparable multiwavelets. She has worked in different projects: "Scattering of Electromagnetic Waves," "Numerical Methods in Nonlinear Optimization," "Applied Harmonic Analysis: Wavelets and Image Processing," "Processing of Remote Sensing Images Generated by Synthetic Aperture Radar and other Sensors."